



# Atropisomeric Hydrogen Bonding Control for CO<sub>2</sub> Binding and Enhancement of Electrocatalytic Reduction at Iron Porphyrins

Philipp Gotico, Loïc Roupnel, Regis Guillot, Marie Sircoglou, Winfried Leibl, Zakaria Halime, Ally Aukauloo

## ► To cite this version:

Philipp Gotico, Loïc Roupnel, Regis Guillot, Marie Sircoglou, Winfried Leibl, et al.. Atropisomeric Hydrogen Bonding Control for CO<sub>2</sub> Binding and Enhancement of Electrocatalytic Reduction at Iron Porphyrins. *Angewandte Chemie International Edition*, 2020, <10.1002/anie.202010859>. <hal-03016806>

**HAL Id: hal-03016806**

**<https://hal.science/hal-03016806v1>**

Submitted on 20 Nov 2020

**HAL** is a multi-disciplinary open access archive for the deposit and dissemination of scientific research documents, whether they are published or not. The documents may come from teaching and research institutions in France or abroad, or from public or private research centers.

L'archive ouverte pluridisciplinaire **HAL**, est destinée au dépôt et à la diffusion de documents scientifiques de niveau recherche, publiés ou non, émanant des établissements d'enseignement et de recherche français ou étrangers, des laboratoires publics ou privés.



HAL Authorization

# Atropisomeric Hydrogen Bonding Control for CO<sub>2</sub> Binding and Electrocatalytic Reduction Enhancement at Iron Porphyrins

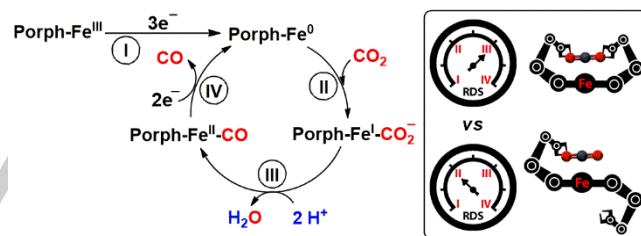
Philipp Gotico,<sup>[a,b]</sup> Loïc Roupnel,<sup>[a]</sup> Régis Guillot,<sup>[a]</sup> Marie Sircoglou,<sup>[a]</sup> Winfried Leibl,<sup>[b]</sup> Zakaria Halime,<sup>\*,[a]</sup> Ally Aukauloo<sup>\*,[a,b]</sup>

**Abstract:** The manipulation of the second coordination sphere for improving the electrocatalytic CO<sub>2</sub> reduction has led to amazing breakthroughs with hydrogen bonding, local proton source, or electrostatic effects. We have developed two atropisomers of an iron porphyrin complex holding two urea functions acting as multiple hydrogen bonding tweezers to lock the metal bound CO<sub>2</sub> in a similar fashion found in the carbon monoxide dehydrogenase (CODH) enzyme. We found that the  $\alpha\alpha$  topological isomer with the two urea groups on the same side of the porphyrin platform provides a stronger binding affinity to tether the incoming CO<sub>2</sub> substrate in comparison to the  $\alpha\beta$  disposition. However, the electrocatalytic activity of the  $\alpha\beta$  atropisomer outperforms its congener with one of the highest reported turnover frequency at low overpotential. The strong H/D KIE observed for the  $\alpha\alpha$  system indicates the existence of a tight water hydrogen bonding network for proton delivery which is disrupted upon addition of exogenous acid source. While the small H/D KIE for the  $\alpha\beta$  isomer and the enhanced electrocatalytic performance upon addition of stronger acid pertain the free access of protons to the bound CO<sub>2</sub> on the opposite side of the urea arm.

Closing the carbon dioxide (CO<sub>2</sub>) cycle by transforming it into fuel in order to mitigate its accumulation in the atmosphere is one of the most important challenges of our fossil-fuel-dependent society.<sup>[1–6]</sup> This solution was inspired by nature itself where green plants efficiently capture sunlight to convert CO<sub>2</sub> and water into various hydrocarbons and O<sub>2</sub> by photosynthesis.<sup>[7,8]</sup> After eons of evolution, the different steps of capture, activation, and transformation of the thermodynamically very stable CO<sub>2</sub> molecule were optimized in sophisticated metalloenzymes.<sup>[9–12]</sup> Similarly, an artificial transformation of CO<sub>2</sub> requires a catalyst that can capture and activate efficiently CO<sub>2</sub> before reducing it in proton-coupled multi-electron processes to skirt the formation of thermodynamically unfavorable high-energy intermediates.<sup>[13]</sup> Principally, the search for homogenous catalysts for CO<sub>2</sub> conversion encompasses noble metals- (Ru, Rh, Pd, Re and Ir) and first-row transition metals- (Mn, Fe, Co,

Ni and Cu) based complexes with mainly nitrogen-based ligands.<sup>[14–18]</sup>

Iron porphyrins are among the most efficient catalysts for CO<sub>2</sub> electrocatalytic reduction (CO<sub>2</sub>ECR) to CO.<sup>[16,19–28]</sup> The simplified mechanism for this reaction can be described in four main steps (Scheme 1) albeit more detailed mechanism with proton-coupled electron transfer processes have also been proposed. Starting from the air-stable **Porph-Fe<sup>III</sup>** oxidation state, the first step is the generation of the catalytically active species **Porph-Fe<sup>0</sup>** by a multiple electron transfer from the electrode to the catalyst. The second step (II) is the substrate (CO<sub>2</sub>) binding to the active **Porph-Fe<sup>0</sup>** followed by the third step (III) where the **Porph-Fe<sup>I</sup>-CO<sub>2</sub><sup>-</sup>** intermediate is protonated twice to yield **Porph-Fe<sup>II</sup>-CO** and a water molecule. In the last step (IV), two electrons are needed to release the reaction product (CO) and regenerate the active species. In this scenario, because they are mainly electron transfer processes, the first (I) and last steps (IV) are considered to be fast at the potential where the electrocatalytic reaction proceeds and do not contribute to the overall rate of the CO<sub>2</sub>ECR.<sup>[29,30]</sup> Therefore, CO<sub>2</sub> binding and proton transfer in



**Scheme 1.** Proposed simplified mechanism for the reduction of CO<sub>2</sub> to CO in iron porphyrins. In this work, we shed light on the importance of controlling the rate-determining step (RDS) in the overall kinetics of the catalytic reaction through architectural second coordination sphere manipulations.

steps II and III respectively are the two processes with a significant contribution to the overall kinetics of the reaction.

[a] Dr. P. Gotico, Loïc Roupnel, Dr. R. Guillot, Dr. M. Sircoglou, Dr. Z. Halime, Prof. A. Aukauloo  
Université Paris-Saclay, CNRS, Institut de chimie moléculaire et des matériaux d'Orsay, 91405, Orsay, France.  
E-mail: zakaria.halime@universite-paris-saclay.fr,  
ally.aukauloo@universite-paris-saclay.fr

[b] Dr. P. Gotico, Dr. W. Leibl, Prof. A. Aukauloo  
Service de Bioénergétique, Biologie Structurale et Mécanismes (SB2SM), CEA/DRF/JOLIOT, Université Paris-Saclay, 91191, Gif-sur-Yvette, France

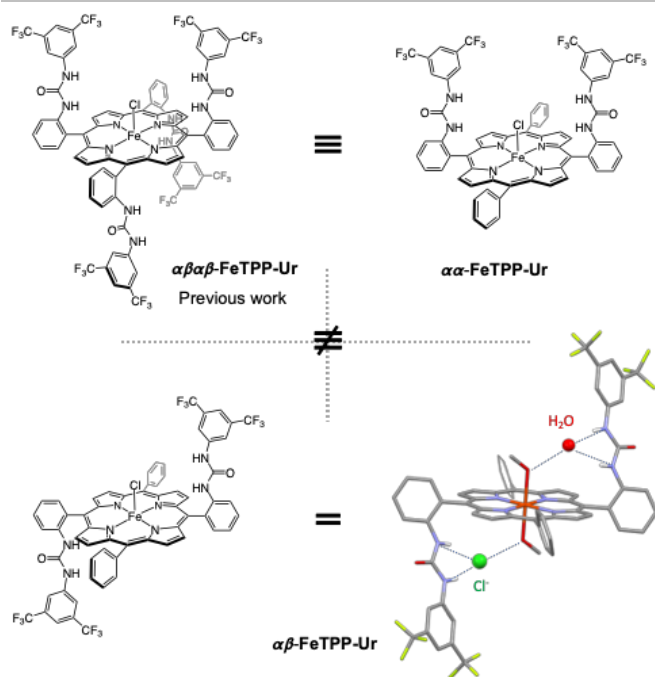


**Figure 1.** Molecular drawings of the previously reported  $\alpha\beta\alpha\beta$ -FeTPP-Ur (top left) and newly synthesized  $\alpha\alpha$ -FeTPP-Ur (top right) and  $\alpha\beta$ -FeTPP-Ur (bottom left). Wireframe and capped sticks representation of  $\alpha\beta$ -FeTPP-Ur X-ray structure (bottom right). Only urea protons are explicitly shown; solvent molecules are omitted for clarity.

The synthetic versatility of tetraarylporphyrins has been determinantal for implementing specific functionalities in the second coordination sphere of the metal center as to replicate the function of cofactors at the active sites of enzymatic systems, for instance, amino acids that directly participate in the breaking and making of bonds. Important breakthroughs in the  $\text{CO}_2\text{ECR}$  rate have been accomplished by adjoining proton relays or cationic groups that resulted in the gain of order of magnitudes in the reactivity pattern of the iron porphyrin catalysts.<sup>[31–34]</sup> A boost of the catalytic reaction rate was also observed when the porphyrin contour was decorated with hydrogen bond donors to improve  $\text{CO}_2$  capture by stabilizing the **Porph-Fe- $\text{CO}_2^-$**  intermediate.<sup>[35,36]</sup> The most flagrant example of such effect on  $\text{CO}_2$  binding rate constant and alongside with a marked repercussion on the rate dependence with the protonation process was observed with a four-pillared porphyrin with urea groups acting as multipoint hydrogen bonding clefts. For this model, we flanked the porphyrin core with substituted urea functions in a face-to-face manner on each side of the molecular plane (noted as  $\alpha\beta\alpha\beta$ -FeTPP-Ur in Figure 1).<sup>[37]</sup> Inspired by subtle dissymmetric functional features encompassing the catalytic enzymatic site of CODH, *i.e.* substrate binding and proton channel, our curiosity was driven to interrogate how the topological arrangement of the urea groups, the hydrogen bonding tweezers, may affect the  $\text{CO}_2\text{ECR}$ . Our underlying target is to have only one set of hydrogen bond donor to participate in the stabilization process, leaving one side of the metal bound  $\text{CO}_2$  free upon activation. We have developed two porphyrin ligand sets holding only two urea groups (Figure 1). For the  $\alpha\alpha$  configuration, the two urea groups are disposed in a face-to-face fashion on the same side of the porphyrinic plane while for the  $\alpha\beta$  configuration these groups are set in trans manner on both sides of the tetrapyrrolic macrocycle (see Figure

1). We found that this subtle modification of the second coordination sphere of the iron porphyrin complexes induces a switch from a catalyst with high affinity for  $\text{CO}_2$  binding for the  $\alpha\alpha$  model to an  $\alpha\beta$  catalyst with a lesser binding aptitude for  $\text{CO}_2$  but importantly with one of the highest turnover frequency (TOF) reported in the literature for  $\text{CO}_2\text{ECR}$  to CO. In what follows we provide experimental and theoretical supports to explain these compounded results in the management of the binding of the  $\text{CO}_2$  and the proton delivery.

Catalysts  $\alpha\alpha$ -FeTPP-Ur and  $\alpha\beta$ -FeTPP-Ur were prepared using previously reported procedures for the  $\alpha\beta\alpha\beta$ -FeTPP-Ur catalyst but starting from the two atropisomers ( $\alpha\alpha$  and  $\alpha\beta$ ) of the 5,15-bis-(2-aminophenyl)-10,20-bis-(phenyl)-porphyrin. The synthetic procedures (Figure S1) and characterization (Figures S22 to S35) of the studied complexes are gathered in the Supplementary Information (SI). Our synthetic design was guided to keep the global chemical formulation of the ligand sets unchanged while maintaining a similar inherent withdrawing inductive effect from two urea groups on the porphyrin cycle. X-ray diffraction analysis of catalyst  $\alpha\beta$ -FeTPP-Ur were performed on single crystals grown by slow evaporation of a solvent mixture (MeOH/ $\text{H}_2\text{O}$ , 4:1) (Figure 1 and see Table S4 for a more detailed description of the structure). The X-ray structure of  $\alpha\beta$ -FeTPP-Ur, as well as that of its corresponding ligand (Figure S20), confirms the  $\alpha\beta$  disposition of the tethered Ur arms on the periphery of the porphyrin skeleton. No crystal of sufficient quality were obtained for the  $\alpha\alpha$ -FeTPP-Ur derivative but the layout of the urea groups should resemble to the previous reported X-ray structure of the  $\alpha\beta\alpha\beta$ -FeTPP-Ur.<sup>[37]</sup> Some interesting structural features are to be noted from the crystallographic structure of  $\alpha\beta$ -FeTPP-Ur. Unlike most of the chloro Fe(III) porphyrinato where the strong binding  $\text{Cl}^-$  sits on the metal ion, herein the  $\text{Cl}^-$  ligand is knocked out of the metal coordination site through strong hydrogen bonding interactions with the NH functions of the urea groups. The axial positions are then filled by two weakly coordinating solvent methanol molecules. The iron center is located within the molecular plane of the porphyrin, a coordination scheme found for low spin hexacoordinated iron (III) complexes with a set of Fe-N bond lengths in the range of 2.04 Å. A crystallization water molecule relays the hydrogen bonding interactions between one bound MeOH and the NH groups of the urea.<sup>[38]</sup> The overlay of the structures of the  $\alpha\beta$ -FeTPP-Ur and the metal-free ligand (Figure S21) depicts minimal overall structural changes for both the urea arms and the porphyrin macrocycle pertaining that the frame of the catalyst can adapt the binding of small molecules with a minimal reorganization energy.

In argon-degassed DMF containing 0.1 M of tetra-N-butylammonium hexafluorophosphate ( $[\text{Bu}_4\text{N}]\text{PF}_6$ ), both catalysts  $\alpha\alpha$ -FeTPP-Ur and  $\alpha\beta$ -FeTPP-Ur show three reversible redox waves corresponding to the formal  $\text{Fe}^{\text{III/II}}$ ,  $\text{Fe}^{\text{II/I}}$ , and  $\text{Fe}^{\text{I/0}}$  couples (Figure 2a, Table S1). As expected, due to the withdrawing inductive effect of the two urea groups, the redox potentials of these three waves are located in between those of the corresponding waves of the nonfunctionalized iron porphyrin (FeTPP) and the  $\alpha\beta\alpha\beta$ -FeTPP-Ur with four urea groups. The only significant difference in the electrochemical response between the two catalysts is a 53 mV cathodic shift of the third wave ( $\text{Fe}^{\text{I/0}}$  couple) for the  $\alpha\beta$ -FeTPP-Ur compared to the  $\alpha\alpha$ -FeTPP-Ur. This could be attributed to the difference in the dipole moment of the two isomers inducing a less optimal orientation of the former porphyrin toward the electrode and thus less favorable electron transfer process (Figure S36).

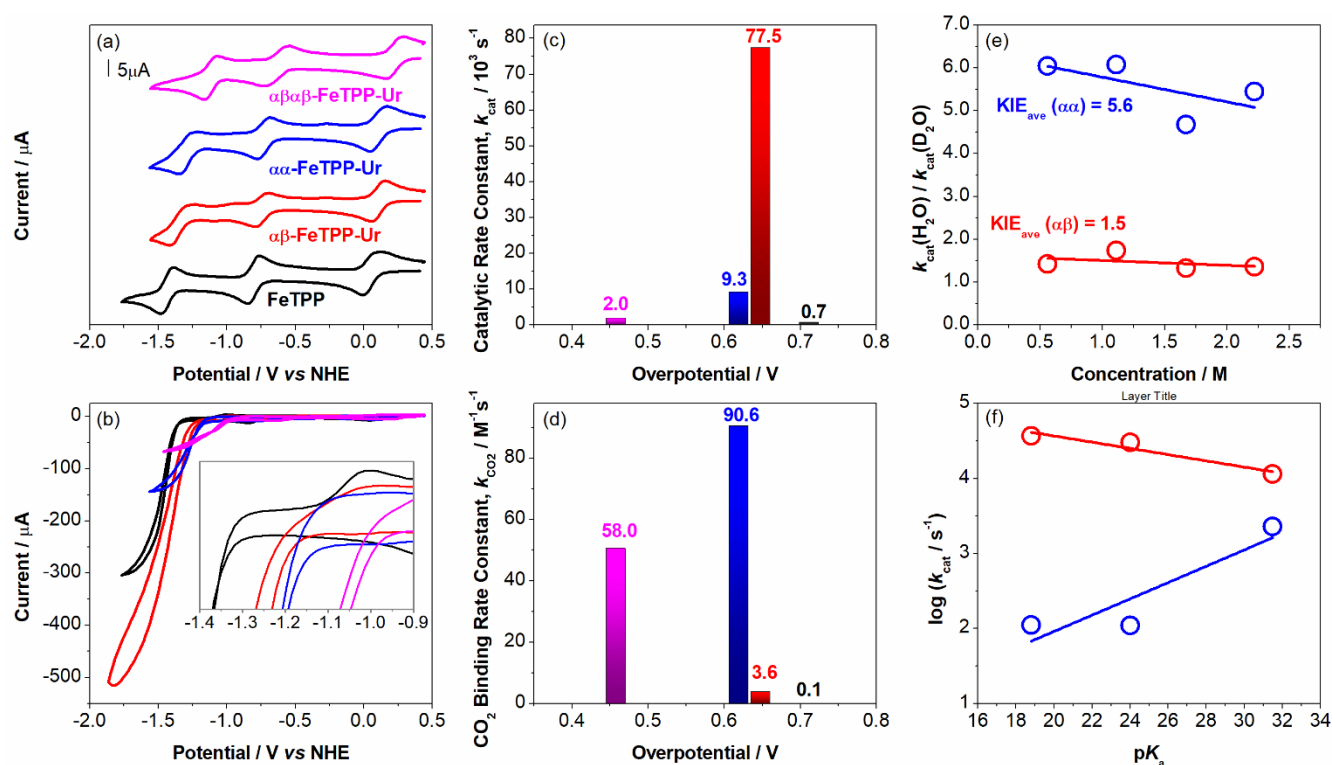


**Figure 2.** (a) Cyclic voltammograms of modified iron porphyrin complexes under investigation:  $\alpha\beta\alpha\beta$ -FeTPP-Ur (magenta),  $\alpha\alpha$ -FeTPP-Ur (blue),  $\alpha\beta$ -FeTPP-Ur (red), and the nonfunctionalized FeTPP (black), at a concentration of 1 mM in dimethylformamide (DMF) containing 0.1 M [Bu<sub>4</sub>N]PF<sub>6</sub> at 25 °C under argon and (b) under CO<sub>2</sub> with 2.22 M water as proton source (inset shows the onset of the catalytic waves). Comparison of (c) the catalytic rate constant, calculated from FOW analysis and (d) the CO<sub>2</sub> binding rate constant as a function of catalytic overpotentials of the modified catalysts. (e) Kinetic Isotope Effect (KIE) when using H<sub>2</sub>O/D<sub>2</sub>O as a proton source for the catalytic CO<sub>2</sub> reduction. (f) Relationship between the catalytic rate constant,  $k_{\text{cat}}$ , as a function of the  $\text{pK}_a$  of the proton source (at 0.28 M concentration). All color legends for (b) to (f) correspond to the same indications as in (a). Calculations and further details are reported in the SI.

In catalytic conditions, *i.e.* under a CO<sub>2</sub> atmosphere and in presence of 2.22 M of H<sub>2</sub>O as a proton source, the difference between the two catalysts becomes more apparent with  $\alpha\beta$ -FeTPP-Ur displaying a much more intense catalytic current for the two-electron reduction of CO<sub>2</sub> to CO than  $\alpha\alpha$ -FeTPP-Ur (Figure 2b). The  $\alpha\beta$ -FeTPP-Ur displays an even more intense catalytic current than that of FeTPP which has more than 130 mV more negative onset catalytic potential. This indicates that  $\alpha\beta$ -FeTPP-Ur has a higher rate for the electrocatalytic reduction of CO<sub>2</sub>. The Foot-of-the-Wave (FOW) analysis of the catalytic currents confirmed this initial observation with almost one order of magnitude higher reaction rate constant for  $\alpha\beta$ -FeTPP-Ur ( $k_{\text{cat}} = 7.75 \times 10^4 \text{ s}^{-1}$ ) than that of  $\alpha\alpha$ -FeTPP-Ur ( $k_{\text{cat}} = 9.25 \times 10^3 \text{ s}^{-1}$ ) and two orders of magnitude higher than that of FeTPP ( $k_{\text{cat}} = 7.46 \times 10^2 \text{ s}^{-1}$ ) (Figure 2c). Electrolysis experiments show that both catalysts display a stable average catalytic current density of 2.57 mA cm<sup>-2</sup> and 4.35 mA cm<sup>-2</sup> with an exclusive production of CO at faradic efficiencies of 92% and 93% for  $\alpha\alpha$ -FeTPP-Ur and  $\alpha\beta$ -FeTPP-Ur, respectively (Figure S11 – S12).

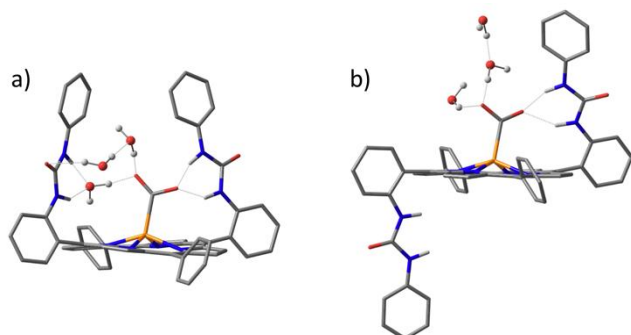
The binding constant for CO<sub>2</sub> at the reactive Fe(0) species was obtained by analysis of the CVs run under argon and in dry DMF. For  $\alpha\alpha$ -FeTPP-Ur where the molecular clamp drawn by the two urea groups on the same side of the porphyrin platform is conserved, the observed CO<sub>2</sub> binding rate constant is as high as  $k_{\text{CO}_2} = 90.6 \text{ M}^{-1} \text{ s}^{-1}$  (Figures 2d and S14) in comparison to  $k_{\text{CO}_2}$  of 58.0 M<sup>-1</sup>s<sup>-1</sup> for  $\alpha\beta\alpha\beta$ -FeTPP-Ur (Figure S16) and  $k_{\text{CO}_2} = 0.1 \text{ M}^{-1} \text{ s}^{-1}$  for FeTPP (Figure S17). We assigned this to the more pronounced nucleophilic character of the Porph-Fe<sup>0</sup> species

(generated at a more negative potential) for the  $\alpha\alpha$ -FeTPP-Ur than the  $\alpha\beta\alpha\beta$ -FeTPP-Ur. However, having only one available urea arm on each side of the porphyrin plane in the case of the  $\alpha\beta$ -FeTPP-Ur atropisomer causes a remarkable drop in the ability of the Porph-Fe<sup>0</sup> species for CO<sub>2</sub> binding with a rate constant of only  $k_{\text{CO}_2} = 3.9 \text{ M}^{-1} \text{ s}^{-1}$  (Figures 2d and S15). Of note, this value is still one order of magnitude higher than the nonfunctionalized FeTPP, indicating the need for the urea arms for improved CO<sub>2</sub> binding. Our DFT calculations outcome also support these experimental facts. Indeed, a higher binding enthalpy and entropic effect were found when two urea clefts grip the metal bound CO<sub>2</sub> as compared to a single binding unit (Table S9).

These counter intuitive results on the binding aptitudes towards CO<sub>2</sub> compared to the corresponding catalytic rate constants of these two atropisomers led to further investigation to provide a rationale for these findings. We have measured a 5.6 normal kinetic isotope effect (KIE) for the electrocatalytic reduction of CO<sub>2</sub> by  $\alpha\alpha$ -FeTPP-Ur with H<sub>2</sub>O/D<sub>2</sub>O as a proton source indicating that proton transfer is involved in the rate determining step (Figures 2e and S18 and Table S3). This value is particularly elevated in comparison to values ca. 1.5 – 2.5 commonly found for the CO<sub>2</sub> reduction with different proton sources (H<sub>2</sub>O, trifluoroethanol, phenol, and acetic acid) and is similar to the one observed for  $\alpha\beta\alpha\beta$ -FeTPP-Ur.<sup>[29,35]</sup> Such an important KIE translates the presence of a tight hydrogen bonding network implicated in the proton transfer process. Hint for this argument comes from the X-ray studies where for both systems we found that a water molecule of crystallization was



lodged within the urea binding cleft. Hence, this result backs the important dependence of the reaction rate on the protonation process (Step III in Scheme 1). Unlike its two analogues,  $\alpha\beta$ -



**FeTPP-Ur** displays a smaller KIE = 1.5 (Figures 2e and S19 and Table S3). This result combined with the fact that  $\alpha\beta$ -**FeTPP-Ur** has a significantly higher overall reaction rate indicates that the proton transfer became in this case a much faster process. Such an observation reflects the structure/reactivity relationship of our designed models whereby for the  $\alpha\beta$  system in contrast with the

**Figure 3.** Notional structures showing distinct proton delivery pathways depending on the atropisomer: a) through a water-cluster disrupting the urea-CO<sub>2</sub> binding, b) via free H<sub>2</sub>O approach (C-bonded hydrogen omitted for clarity)

$\alpha\alpha$ , the lack of a urea arm opens the way for the rapid convey of protons to the “loose” oxygen atom of the metal bound CO<sub>2</sub> under electrochemical reduction process (Figure 3).

We further investigated the effect of the nature of the acid source on the electrocatalytic behavior of both atropisomeric catalysts. We tested more acidic proton sources than water ( $pK_a = 31.5$ ), such as trifluoroethanol (TFE,  $pK_a = 24.0$ ) or phenol (PhOH,  $pK_a = 18.8$ ) to provide common grounds for comparison with the literature. In the case of  $\alpha\alpha$ -**FeTPP-Ur**, our results single out from the common observable trend for such a variation. In effect, we noticed a lowering of the reaction rate upon addition stronger acid (Figure 2f, S8 and S9 and Table S2). Such a particularity pushes forward the scheme of formation of a topological tight hydrogen bonding network containing the water molecules locked by the urea functions and the **Porph-Fe-CO<sub>2</sub>** adduct while the other urea group maintains it in position during the protonation process. Henceforth, the addition of stronger or more sterically hindered acid may hinder the formation or disrupt this network. For the  $\alpha\beta$ -**FeTPP-Ur** the protonation process seems to proceed with a linear dependence of catalytic reaction rate constant with the  $pK_a$  of the acid (Figure 2f, S6 and S7 and Table S2), a classic trend observed for most reported molecular-based electrocatalytic studies.<sup>[29]</sup> Accordingly, protons are conveyed more efficiently with stronger acids to the mono-oxygen locked [**Porph-Fe-CO<sub>2</sub>-Urea**] intermediate through the ‘freely-accessible’ O atom.

Taking inspiration from the dissymmetric topological distribution of second sphere amino acids assisting the catalytic active sites of metalloenzymes, this study, provides an insightful example on how implementing such facets in well-defined molecular catalysts can lead to mitigate the substrate affinity while enhancing the catalytic rates. Considering the process for optimizing the properties of catalysts as the quest for the right set of Goldilocks combination of balanced substrate activation

and destabilization, the present investigation greatly highlights how simple architectural changes can modify the relevant rate-determining step of the catalytic reaction. Such chemical tools are invaluable for chemists to adjust catalyst performances toward more efficient CO<sub>2</sub> capture at low substrate concentration or to favor a faster catalysis at higher CO<sub>2</sub> concentration.

## Experimental Section

Dimethylformamide (DMF, Aldrich 99.9%), tetrabutyl-ammonium hexafluorophosphate ([Bu<sub>4</sub>N]PF<sub>6</sub>, Aldrich 99%) were used as received. All other chemical reagents used in the synthetic route were obtained from commercial sources as guaranteed-grade reagents and used without further purification. Cyclic voltammetry measurements were performed in an electrochemical cell composed of a glassy carbon (3 mm diameter) working electrode, an aqueous standard calomel electrode (SCE) as the reference electrode, and a platinum wire counter electrode using a dimethylformamide (DMF) solvent containing 1 mM catalyst and 0.1 M [Bu<sub>4</sub>N]PF<sub>6</sub>. Bulk electrolysis was performed in a gas-tight two-compartment cell with a glassy carbon working electrode (effective surface area of 1.41 cm<sup>2</sup>), reference electrode (Ag/AgNO<sub>3</sub>), and titanium grid as counter electrode. Products analysis was analyzed using gas chromatography (GC - TraceGC Ultra, ThermoScientific) equipped with a molecular sieve porous layer open tubular (PLOT) column, helium carrier gas, and a thermal conductivity detector (TCD).

## Acknowledgements

This work has been supported by the French National Research Agency (ANR-19-CE05-0020-02, LOCO). We thank CNRS, CEA Saclay, ICMMO and University Paris-Saclay for the financial support. We also thank the synthesis support facility (Pôle Synthèse) at ICMMO for their help with the synthesis of the starting porphyrin platform. Computational work was performed using HPC resources from GENCI-CINES (Grant A0070810977).

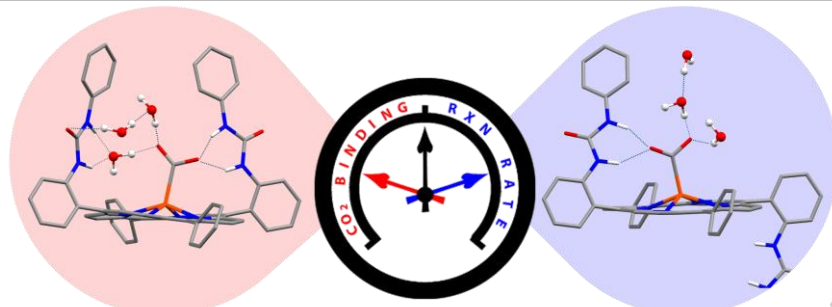
**Keywords:** carbon dioxide reduction • iron porphyrin • hydrogen bonding • urea • second coordination

- [1] O. S. Bushuyev, P. D. Luna, C. T. Dinh, L. Tao, G. Saur, J. van de Lagemaat, S. O. Kelley, E. H. Sargent, *Joule* **2018**, 2, 825–832.
- [2] T. P. Senftle, E. A. Carter, *Acc. Chem. Res.* **2017**, 50, 472–475.
- [3] Q.-L. Zhou, *Angewandte Chemie International Edition* **2016**, 55, 5352–5353.
- [4] M. Aresta, A. Dibenedetto, A. Angelini, *Chem. Rev.* **2014**, 114, 1709–1742.
- [5] S. C. Roy, O. K. Varghese, M. Paulose, C. A. Grimes, *ACS Nano* **2010**, 4, 1259–1278.
- [6] G. A. Olah, *Angewandte Chemie International Edition* **2005**, 44, 2636–2639.
- [7] R. L. House, N. Y. M. Iha, R. L. Coppo, L. Alibabaei, B. D. Sherman, P. Kang, M. K. Brennaman, P. G. Hoertz, T. J. Meyer, *Journal of Photochemistry and Photobiology C: Photochemistry Reviews* **2015**, 25, 32–45.
- [8] D. G. Nocera, *Acc. Chem. Res.* **2017**, 50, 616–619.
- [9] J. Barber, *Chem. Soc. Rev.* **2008**, 38, 185–196.
- [10] J.-H. Jeoung, H. Dobbek, *Science* **2007**, 318, 1461.
- [11] A. M. Appel, J. E. Bercaw, A. B. Bocarsly, H. Dobbek, D. L. DuBois, M. Dupuis, J. G. Ferry, E. Fujita, R. Hille, P. J. A. Kenis, C. A. Kerfeld, R. H. Morris, C. H. F. Peden, A. R. Portis, S. W. Ragsdale, T. B. Rauchfuss, J. N. H. Reek, L. C. Seefeldt, R. K. Thauer, G. L. Waldrop, *Chem. Rev.* **2013**, 113, 6621–6658.

- [12] M. Can, F. A. Armstrong, S. W. Ragsdale, *Chem. Rev.* **2014**, *114*, 4149–4174.
- [13] J. Schneider, H. Jia, J. T. Muckerman, E. Fujita, *Chem. Soc. Rev.* **2012**, *41*, 2036–2051.
- [14] R. Francke, B. Schille, M. Roemelt, *Chem. Rev.* **2018**, *118*, 4631–4701.
- [15] F. Wang, *ChemSusChem* **2017**, *10*, 4393–4402.
- [16] H. Takeda, C. Cometto, O. Ishitani, M. Robert, *ACS Catal.* **2017**, *7*, 70–88.
- [17] M. Cokoja, C. Bruckmeier, B. Rieger, W. A. Herrmann, F. E. Kühn, *Angewandte Chemie International Edition* **2011**, *50*, 8510–8537.
- [18] N. Elgrishi, M. B. Chambers, X. Wang, M. Fontecave, *Chem. Soc. Rev.* **2017**, *46*, 761–796.
- [19] K. Takahashi, K. Hiratsuka, H. Sasaki, S. Toshima, *Chem. Lett.* **1979**, *8*, 305–308.
- [20] M. Hammouche, D. Lexa, M. Momenteau, J. M. Saveant, *J. Am. Chem. Soc.* **1991**, *113*, 8455–8466.
- [21] C. Costentin, J.-M. Savéant, *Nat. Rev. Chem.* **2017**, *1*, 0087.
- [22] A. W. Nichols, C. W. Machan, *Front. Chem.* **2019**, *7*, 397.
- [23] K. E. Dalle, J. Warnan, J. J. Leung, B. Reuillard, I. S. Karmel, E. Reisner, *Chem. Rev.* **2019**, *119*, 2752–2875.
- [24] C.-F. Leung, P.-Y. Ho, *Catalysts* **2019**, *9*, 760.
- [25] F. Franco, S. Fernández, J. Lloret-Fillol, *Curr Opin Electrochem* **2019**, *15*, 109–117.
- [26] P. Gotico, Z. Halime, A. Aukauloo, *Dalton Trans.* **2020**, *49*, 2381–2396.
- [27] I. Bhugun, D. Lexa, J.-M. Saveant, *J. Am. Chem. Soc.* **1994**, *116*, 5015–5016.
- [28] I. Bhugun, D. Lexa, J.-M. Savéant, *J. Am. Chem. Soc.* **1996**, *118*, 1769–1776.
- [29] C. Costentin, S. Drouet, G. Passard, M. Robert, J.-M. Savéant, *J. Am. Chem. Soc.* **2013**, *135*, 9023–9031.
- [30] A. J. Sathrum, C. P. Kubiak, *J. Phys. Chem. Lett.* **2011**, *2*, 2372–2379.
- [31] C. Costentin, S. Drouet, M. Robert, J.-M. Savéant, *Science* **2012**, *338*, 90–94.
- [32] C. Costentin, G. Passard, M. Robert, J.-M. Savéant, *Proc. Natl. Acad. Sci. USA* **2014**, *111*, 14990–14994.
- [33] C. Costentin, M. Robert, J.-M. Savéant, A. Tatin, *Proc. Natl. Acad. Sci. USA* **2015**, *112*, 6882–6886.
- [34] G. Neri, I. M. Aldous, J. J. Walsh, L. J. Hardwick, A. J. Cowan, *Chem. Sci.* **2016**, *7*, 1521–1526.
- [35] E. M. Nichols, J. S. Derrick, S. K. Nistanaki, P. T. Smith, C. J. Chang, *Chem. Sci.* **2018**, *9*, 2952–2960.
- [36] P. Sen, B. Mondal, D. Saha, A. Rana, A. Dey, *Dalton Trans.* **2019**, *48*, 5965–5977.
- [37] P. Gotico, B. Boitrel, R. Guillot, M. Sircoglou, A. Quaranta, Z. Halime, W. Leibl, A. Aukauloo, *Angew. Chem. Int. Ed* **2019**, *58*, 4504–4509.
- [38] F. A. Walker, U. Simonis, in *Encyclopedia of Inorganic and Bioinorganic Chemistry*, American Cancer Society, **2011**.
- [39] Y. Fang, M. O. Senge, E. Van Caemelbecke, K. M. Smith, C. J. Medforth, M. Zhang, K. M. Kadish, *Inorg. Chem.* **2014**, *53*, 10772–10778.
- [40] J. A. Hodge, M. G. Hill, H. B. Gray, *Inorg. Chem.* **1995**, *34*, 809–812.

## Entry for the Table of Contents

## COMMUNICATION



**Hold me but not too tight!** Adapting the 3D topological layout of an iron porphyrin catalyst bearing urea groups as multipoint hydrogen bonding donors in the second sphere can induce a switch from higher affinity for CO<sub>2</sub> binding to faster reaction

*Philipp Gotico, Loïc Roupnel, Régis Guillot, Marie Sircoglou, Winfried Leibl, Zakaria Halime, \* Ally Aukauloo\**

**Page No. – Page No.**

**Atropisomeric Hydrogen Bonding Control for CO<sub>2</sub> Binding and Electrocatalytic Reduction Enhancement at Iron Porphyrins**